ARTICLE NO. 78-1270R

Control Law Synthesis for Active Flutter Suppression Using Optimal Control Theory

Jerry R. Newsom*
NASA Langley Research Center, Hampton, Va.

This paper describes a study investigating the use of optimal control theory for the synthesis of an active flutter-suppression control law. For an example design application, a high-aspect-ratio cantilever wind-tunnel wing model is considered. The structural dynamics are represented by analytically computed natural frequencies and mode shapes. The three-dimensional unsteady aerodynamic forces for oscillatory motion are computed employing the doublet-lattice technique. With the aid of finite-order approximating functions for representing the aerodynamic forces in the time domain, the "flutter equations" are written in the standard state vector form. Linear optimal control theory is then applied to find particular sets of gain values which minimize a quadratic cost function of the states and controls. These control laws are shown to increase the flutter dynamic pressure by at least 50% at Mach numbers 0.7 and 0.9. The closed-loop system's control surface activity in a gust environment is also examined.

Nomenclature

c = reference length
$h(x,y,t)$ = vertical displacement
$H_R(\omega)$ = frequency response function of Rth response
i = $\sqrt{-1}$
J = cost function
k = reduced frequency = $c\omega/2U$
K_i = generalized stiffness for ith vibration mode
$m(x,y)$ = mass distribution
M_i = generalized mass for ith vibration mode
p = dimensionless Laplace variable = $cs/2U$
P_N = Nth pole for aerodynamic curve-fit function
$\bar{q}$ = dynamic pressure = $\frac{1}{2}\rho U^2$
q_i = generalized coordinate for ith mode
Q_i = generalized aerodynamic force for ith mode
s = Laplace variable
S = surface area
t = time
U = freestream velocity
w_g = vertical gust velocity
$Z_i(x,y)$ = deflection of the ith vibration mode at x,y
Z_m = mth zero for aerodynamic curve-fit function
β_m = mth aerodynamic lag term
δ = control surface deflection
$\Delta p(x,y,t)$ = total aerodynamic pressure distribution
Δp_j = pressure distribution for jth mode
Δp_{w_g} = pressure distribution for vertical gust velocity
Δp_δ = pressure distribution for control surface rotation
ω = circular frequency, rad/s
ω_i = natural frequency of ith vibration mode
$\phi w_g(\omega)$ = vertical gust velocity power spectral density
ρ = freestream density
σ_R = rms value of Rth response
σ_{w_g} = rms value of vertical gust velocity
ξ = damping ratio

Matrices

$[A]$ = system dynamics matrix
$[A_i]$ = real aerodynamic coefficients for motion forces
$[B]$ = control distribution matrix
$[D_i]$ = real aerodynamic coefficients for control surface forces
$[F_j]$ = real coefficients for generalized coordinates, open loop
$[\bar{F}_j]$ = real coefficients for generalized coordinates, closed loop
$[G_i]$ = real aerodynamic coefficients for vertical gust velocity forces
$[H]$ = disturbance distribution matrix
$[K]$ = generalized stiffness matrix
$[K^*]$ = feedback gain matrix
$[M]$ = generalized mass matrix
$[P]$ = Riccati solution matrix
$\{q\}$ = generalized coordinate vector
$[Q]$ = state weighting matrix
$[Q_{ij}]$ = matrix representing generalized aerodynamic motion forces
$[Q_{i_{w_g}}]$ = matrix representing generalized aerodynamic gust forces
$[Q_{i_\delta}]$ = matrix representing generalized aerodynamic control surface forces
$[R]$ = control weighting matrix
$[R_j]$ = real coefficients for control surface rotation
$[T_j]$ = real coefficients for vertical gust velocity
$\{u\}$ = control vector
$\{X\}$ = state vector
$\{\eta\}$ = disturbance vector
$(\dot{\cdots})$ = dot superscripts, indicate time derivatives

Presented as Paper 78-1270 at the AIAA Guidance and Control Conference, Palo Alto, Calif., Aug. 7-9, 1978; submitted Aug. 24, 1978; revision received Feb. 12, 1979. Reprints of this article may be ordered from AIAA Special Publications, 1290 Avenue of the Americas, New York, N.Y. 10019. Order by Article No. at top of page. Member price $2.00 each, nonmember, $3.00 each. **Remittance must accompany order.**

Index categories: Aeroelasticity and Hydroelasticity; Guidance and Control; Structural Dynamics.

*Aerospace Engineer, Aeroelastic Optimization Office. Member AIAA.

Introduction

FLUTTER is an aeroelastic self-excited instability in which the airstream energy is absorbed by the lifting surface. The motion is complex and usually consists of both bending and torsional components. With the increased flexibility of the modern-day strength-sized aircraft, the likelihood of flutter within the flight envelope has increased. Aircraft exhibiting this characteristic include the B-52, the U.S. National SST, and the B-1. Preliminary design studies have indicated that weight penalities of as much as an additional 2-4% of the total structural weight would be required to passively (through increased structural stiffness) solve the flutter problem for an SST configuration.[1] Other such

passive methods include mass balancing and speed restrictions. Any of these methods of flutter prevention could result in substantial performance penalties to the aircraft. Therefore, there is a considerable interest in developing better methods of increasing the flutter speed which can be used in place of, or in combination with, the traditional passive methods.

With the recent advances in active control technology, an active flutter-suppression system is now feasible, offering the potential, in many cases, for solving flutter problems with significantly less weight and performance penalties. Active flutter suppression can be defined as the prevention of flutter by using an aerodynamic control surface commanded by signals through an appropriate control law.

The major obstacle in applying optimal control theory to the synthesis of an active flutter-suppression control law is the development of the aeroelastic equations of motion in the form of constant-coefficient differential equations. The reason for this problem is the lack of a theory to represent the unsteady aerodynamics for arbitrary motion in constant-coefficient differential equation form. Vepa[2] and Edwards[3] have been studying this problem. Also, Morino[4] has developed a formulation for three-dimensional unsteady aerodynamics which is valid for arbitrary motion, but the calculated form cannot be used directly in constant-coefficient differential equations.

With the availability of well-developed techniques for computing unsteady aerodynamics for oscillatory motion, Vepa and others have suggested the use of Padé approximates to represent the unsteady aerodynamics for arbitrary motion. A Padé approximate is a rational function which approximates the function in some range of its argument. Vepa used a Padé approximate to Theodorsen's function in developing the equations of motion for the two-dimensional typical section in state vector form.[5]

The purpose of this paper is to present some analytical techniques that are useful for the analysis and synthesis of an active flutter-suppression control law. Optimal regulator solutions are obtained through the solution of the matrix Riccati equation. Results from applying optimal control theory to the design of an active flutter-suppression control law for a cantilever wind-tunnel wing model are presented.

Aeroelastic Modeling

Employing a modal approach, the elastic deformation of the wing is described by a linear combination of the undamped natural vibration modes of the system[6,7]:

$$h(x,y,t) = \sum_{i=1}^{n} Z_i(x,y)\,q_i(t) \tag{1}$$

where $Z_i(x,y)$ is the deflection of the ith mode at x,y. If structural damping is neglected, Lagrange's equations of motion are

$$M_i\ddot{q}_i(t) + K_i q_i(t) = Q_i(t) \qquad (i=1,2,\ldots n) \tag{2}$$

where

M_i	$=\int_S m(x,y)\,Z_i^2(x,y)\,dS$	generalized mass
K_i	$=M_i\omega_i^2$	generalized stiffness
Q_i	$=-\int_S \Delta p(x,y,t)\,Z_i(x,y)\,dS$	generalized aerodynamic force

When small amplitudes are assumed, the total pressure distribution $\Delta p(x,y,t)$ can be expressed as the sum of contributions due to each flexible mode. The control surface pressure distribution is separated and identified as the control input. The gust pressure distribution is treated in a similar manner to the control input:

$$\Delta p(x,y,t) = \sum_{j=1}^{n} \Delta p_j(x,y)\,q_i(t) + \Delta p_\delta(x,y)\,\delta(t) + \Delta p_{w_g}(x,y)\,w_g(t) \tag{3}$$

Substituting Eq. (3) into Eq. (2) yields the following expression for the equations of motion:

$$M_i\ddot{q}_i(t) + \omega_i^2 M_i q_i(t) + \sum_{j=1}^{n} Q_{ij} q_i(t) = -Q_{i_\delta}\delta(t) - Q_{i_{w_g}} w_g(t) \tag{4}$$

The generalized aerodynamic forces for oscillatory motion are computed using the doublet-lattice method of Ref. 8. This method requires the subdivision of the lifting surface into an array of trapezoidal boxes arranged in streamwise columns with a line of doublets located at the quarter chord of each box. The geometric boundary condition of tangential flow is satisfied at the ¾ chord location of each box. Numerical representation of this method is well established in the computer codes developed in Ref. 9.

Padé Approximation

Recently, there has been considerable effort in developing techniques which use information from the oscillatory aerodynamic forces to generate approximations capable of continuation into the complex frequency or Laplace s-plane.[2,3] Perhaps the technique that has received the most attention, at least for three-dimensional aerodynamics, is the Padé approximation. With this technique, each generalized aerodynamic force is approximated by means of a Padé approximate, that is, a rational function of a finite-degree polynomial in the complex transform variable p. The order of the Padé approximate is the highest power of p in the denominator polynomial. As this order is increased, the fit of the original oscillatory data will usually become better. However, the increased accuracy can be offset by the resulting higher-order models.

The Padé approximate technique involves curve-fitting a mathematical function of ik to the aerodynamic forces which consist of real and imaginary parts that are functions of discrete values of k.

Various forms of mathemtical functions can be employed to fit the data. Examples include

$$[Q(ik)] = [A_0] + [A_1](ik) + [A_2](ik)^2 + [A_3](ik)^3 \ldots \tag{5}$$

$$[Q(ik)] = \sum_{m=1}^{M} (Z_m + ik) \Big/ \sum_{n=1}^{N} (P_n + ik) \tag{6}$$

$$[Q(ik)] = [A_0] + [A_1](ik) + [A_2](ik)^2 + \sum_{m=1}^{L} \frac{[A_{m+2}](ik)}{\beta_m + (ik)} \tag{7}$$

The form of Eq. (7), with one denominator term, was employed in this study. The aerodynamic lag term β, which is assumed to be a known constant, was selected to be the uncontrolled flutter reduced frequency. Using Eq. (7), a set of least-squares curve-fit equations can be formulated for both the real and imaginary parts of the generalized aerodynamic forces. These equations can be solved for the A_0, A_1, A_2, and A_3 matrices. The form of Eq. (7) was employed to fit all of the wing motion, control surface, and gust aerodynamic forces. This procedure is similar to that described in Ref. 10.

State Space Equations of Motion

State space representation consists of a set of first-order simultaneous differential equations of the form

$$\dot{X}(t) = f[X(t),u(t),t] \tag{8}$$

Here t is the time variable, $X(t)$ is a real n-dimensional column vector which is the state of the system, and $u(t)$ is a real m-dimensional column vector which is the input variable or control variable.

By using the aerodynamic approximating coefficients in Eq. (7), the equations of motion are

$$\left\{[M]s^2+[K]+\tfrac{1}{2}\rho U^2\{[A_0]+(c/2U)[A_1]s+(c/2U)^2[A_2]s^2+\frac{(c/2U)[A_3]s}{(c/2U)s+\beta}\}\right\}\{q(s)\}$$
$$=\tfrac{1}{2}\rho U^2\left\{[D_0]+(c/2U)[D_1]s+(c/2U)^2[D_2]s^2+\frac{(c/2U)[D_3]s}{(c/2U)s+\beta}\right\}\delta(s)+\tfrac{1}{2}\rho U\left\{[G_0]+(c/2U)[G_1]s+(c/2U)^2[G_2]s^2+\frac{(c/2U)[G_3]s}{(c/2U)s+\beta}\right\}w_g(s) \tag{9}$$

Multiplying through by the denominator term yields a matrix polynomial in s of the form

$$\{[F_0]+[F_1]s+[F_2]s^2+[F_3]s^3\}\{q(s)\}=\{[R_0]+[R_1]s+[R_2]s^2+[R_3]s^3\}\delta(s)+\{[T_0]+[T_1]s+[T_2]s^2+[T_3]s^3\}w_g(s) \tag{10}$$

All of the above matrices are functions of velocity and density for a specific Mach number. With zero initial conditions, the differential equations that describe the system can be reconstructed by identifying derivatives with the powers of s, so that in the time domain the equations are

$$[F_3]\{\dddot{q}\}+[F_2]\{\ddot{q}\}+[F_1]\{\dot{q}\}+[F_0]\{q\}=[R_3]\dddot{\delta}+[R_2]\ddot{\delta}+[R_1]\dot{\delta}+[R_0]\delta+[T_3]\dddot{w}_g+[T_2]\ddot{w}_g+[T_1]\dot{w}_g+[T_0]w_g \tag{11}$$

One must note that the order of the equations is very dependent upon the approximation for the aerodynamic forces. The differential Eq. (11) can be cast in state space form by the following substitutions:

$$\{X_1\}=\{q\}$$
$$\{X_2\}=\{\dot{q}\}$$
$$\{X_3\}=\{\ddot{q}\}$$

Employing these substitutions, Eq. (11) can be cast into the following state space representation:

$$\{\dot{X}\}=[A]\{X\}+[B]\{u\}+[H]\{\eta\} \tag{12}$$

where

$$\{X\}=[q,\ldots q_n\dot{q},\ldots\dot{q}_n\ddot{q},\ldots\ddot{q}_n]^T$$
$$\{u\}=[\delta\ \dot{\delta}\ \ddot{\delta}\ \dddot{\delta}]^T$$
$$\{\eta\}=[w_g\dot{w}_g\ddot{w}_g\dddot{w}_g]^T$$

The elements of the state vector are seen to be the generalized coordinates and their first and second time derivatives. The u and η vectors consist of the control surface displacement, gust velocity, and their derivatives.

Control System Synthesis

For this study, the synthesis procedure is treated as a deterministic regulator problem. The function to be minimized is an infinite time integral quadratic criterion in terms of the states and the controls:

$$J=\int_0^\infty (X^TQX+u^TRu)\,dt \tag{13}$$

where Q and R are weighting matrices on the states and controls. The minimization of this performance function leads to the optimal control law[11]

$$u=K^*X \tag{14}$$

$$K^*=R^{-1}B^TP \tag{15}$$

where P is the steady-state solution of the matrix Riccati equation:

$$-\dot{P}=PA+A^TP-PR^{-1}B^TP+Q \tag{16}$$

The application of quadratic optimization is an iterative process of selecting the appropriate performance function through changes in the weighting matrices Q and R. The choice of the weights is expedited by the designer's past experience and his understanding of the physics of the problem.

Frequency Response Power Spectral Density (PSD) Techniques

PSD techniques use random process theory to predict statistical properties of the system's responses to random gust disturbances through the frequency response functions. The frequency response functions describe the system's responses to sinusoidally varying atmospheric turbulence.[12,13] The statistical property of interest in this study is the root mean square (rms) value of the control surface displcement and rate in a unit vertical gust field. The rms value of a response σ_R, per unit rms gust velocity, σ_{w_g}, is given by the following expression:

$$\frac{\sigma_R}{\sigma_{w_g}}=\left[\frac{\int_0^\infty |H_R(\omega)|^2\phi w_g(\omega)\,d\omega}{\int_0^\infty \phi w_g(\omega)\,d\omega}\right]^{1/2} \tag{17}$$

The atmospheric turbulence PSD function used in this study is the von Karman[12] power spectrum with a characteristic gust length of 762 m.

The frequency response functions are formulated through Eq. (10):

$$[F(s)]\{q(s)\}=[R(s)]\delta(s)+[T(s)]w_g(s) \tag{18}$$

Since the states are the generalized coordinates and their derivatives, the optimal gains can be implemented into Eq. (18) through the following equation:

$$\delta(s)=\sum_{i=1}^{n}K_i^*q(s)+\sum_{i=n+1}^{2n}K_i^*sq(s)+\sum_{i=2n+1}^{3n}K_i^*s^2q(s) \tag{19}$$

Substituting Eq. (19) into Eq. (18) yields a set of equations of the following form:

$$[\bar{F}(s,K^*)]\{q(s)\}=[G(s)]w_g(s) \tag{20}$$

The $\bar{F}$ matrix is now a function of the gain values K_i^*. Letting $s=i\omega$, Eq. (20) can be solved at discrete frequency points for the generalized coordinate frequency-response functions. The integral of Eq. (17) is numerically evaluated using a Gauss-Legendre Quadrature formula with the upper limit of integration 1.5 times the highest mode frequency.

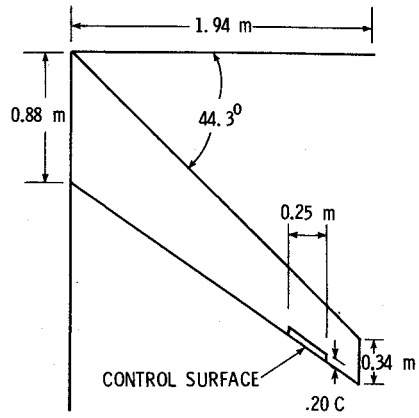

Fig. 1 Planform geometry (all linear dimensions in meters).

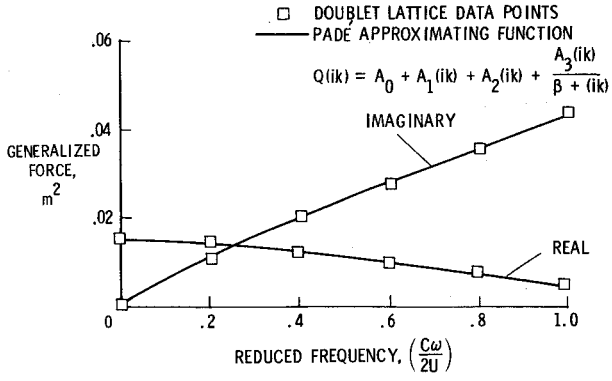

Fig. 2 Aerodynamic curve fit.

Numerical Results

The example problem used in this study is a cantilever wind-tunnel model wing that represents the vehicle described in Ref. 14. The wing has one 20% chord outboard trailing-edge control surface. A planform drawing showing the control surface location is shown in Fig. 1.

Equations of motion are generated using the first five natural vibration modes as generalized coordinates. The generalized coordinates cover a frequency range from 5.92 Hz to 59.30 Hz.

In order to compute the generalized aerodynamic force matrices, the doublet-lattice procedure requires the subdivision of the planform geometry into small trapezoidal "boxes." The wing is represented by 119 boxes with eight boxes modeling the control surface. The generalized aerodynamic force matrices are calculated for six values of reduced frequency ($k = 0.0$, 0.2, 0.4, 0.6, 0.8, 1.0) and two Mach numbers (0.7 and 0.9).

A computer program was employed to obtain the least-squares curve fit to the oscillatory data. Fig. 2 shows a comparison between the original oscillatory data and the approximating function for a representative element of the generalized force matrix.

At this point the control and disturbance vectors consist of the control rotation, gust velocity, and their derivatives. For the purposes of this study, the aerodynamic forces proportional to the derivatives of the control rotation and gust velocity are neglected. However, if one knows, for example, the dynamic equations that relate the derivatives of the control rotation to the control rotation (actuator dynamics), these aerodynamic forces could, and perhaps should, be included. However, the overall design process would be basically the same.

The state equations formulated are functions of Mach number, velocity and density. For a given Mach number, the velocity is fixed by the speed of sound in the wind tunnel. By fixing Mach number and therefore velocity (i.e., a match point), the characteristic roots can be found for a series of dynamic pressures by increasing density. The dynamic pressure at which the real part of one of the roots becomes zero is the flutter dynamic pressure and the imaginary part is the flutter frequency. The roots can then be used to construct a dynamic pressure ($\bar{q}$) root locus. Figures 3 and 4 show the dynamic pressure root loci for Mach numbers 0.9 and 0.7, respectively. At Mach 0.9, the flutter dynamic pressure is predicted to be 5.003 kPa at a frequency of 70.0 rad/s. At Mach 0.7, the flutter dynamic pressure is predicted to be 6.368 kPa at a frequency of 72.5 rad/s. Conventional flutter analyses performed by the author predict the flutter dynamic pressures to be 4.908 kPa (Mach 0.9) and 6.512 kPa (Mach 0.7). The classical wing flutter behavior is indicated since the frequencies of primary wing bending (mode 1) and primary wing torsion (mode 2) coalesce with increasing dynamic pressure.

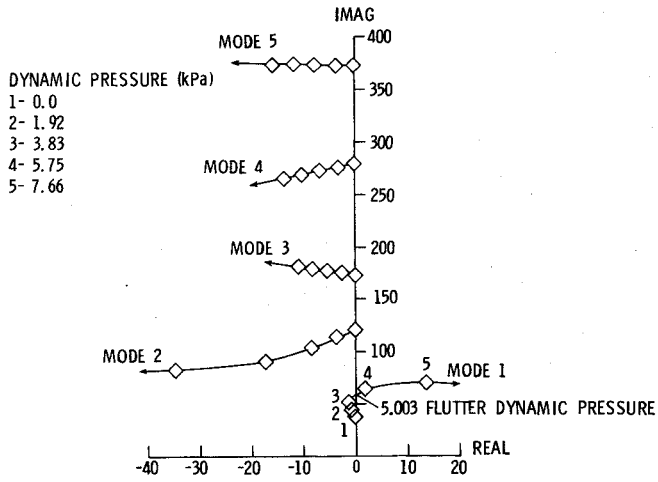

Fig. 3 Open-loop $\bar{q}$ root locus, Mach 0.9.

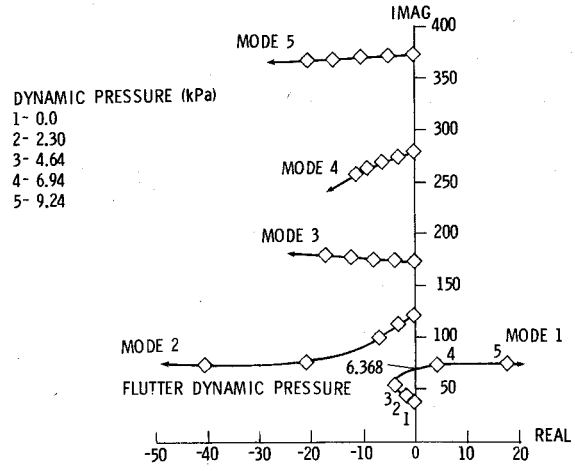

Fig. 4 Open-loop $\bar{q}$ root locus, Mach 0.7.

To assess the performance of the control laws synthesized using optimal control theory, the maximum allowable rms control surface displacement and rate must be established. The maximum allowable rms displacement and rate are chosen to be 6.57 deg. and 656.60 deg/s, respectively, for a 1 m/s rms gust velocity. As indicated in Ref. 15, this allows actuation systems to be sized for linear operation for a 1.83 m/s rms gust velocity.

The goals selected for the flutter-suppression control law are to increase the flutter dynamic pressure by 50%, and at

Table 1 Open-loop eigenvalues at design condition

	Mach 0.9		Mach 0.7	
No.	Real	Imaginary	Real	Imaginary
1	13.909	70.004	19.742	73.050
2	13.909	−70.004	19.742	−73.050
3	−34.916	82.734	−44.139	71.282
4	−34.916	−82.734	−44.139	−71.282
5	−10.836	180.614	−18.186	179.110
6	−10.836	−180.614	−18.186	−179.110
7	−13.645	264.739	−11.632	256.692
8	−13.645	−264.739	−11.632	−256.692
9	−15.775	373.305	−21.729	367.315
10	−15.775	−373.305	−21.729	−367.315
11	−43.742	0.0	−35.667	0.0
12	−55.903	0.0	−44.384	0.0
13	−56.721	0.0	−44.658	0.0
14	−57.351	0.0	−44.836	0.0
15	−59.706	0.0	−46.212	0.0

Table 2 Closed-loop eigenvalues using full-state feedback gains at design condition

	Mach 0.9		Mach 0.7	
No.	Real	Imaginary	Real	Imaginary
1	−13.909	70.004	−19.742	73.050
2	−13.909	−70.004	−19.742	−73.050
3	−34.916	82.734	−44.139	71.282
4	−34.916	−82.734	−44.139	−71.282
5	−10.836	180.614	−18.186	179.110
6	−10.836	−180.614	−18.186	−179.110
7	−13.645	264.739	−11.632	−256.692
8	−13.645	−264.739	−11.632	−256.692
9	−15.775	373.305	−21.729	367.315
10	−15.774	−373.305	−21.729	−367.315
11	−43.742	0.0	−35.667	0.0
12	−55.903	0.0	−44.384	0.0
13	−56.721	0.0	−44.658	0.0
14	−57.351	0.0	−44.836	0.0
15	−59.706	0.0	−46.212	0.0

Table 3 Closed-loop eigenvalues using partial-state feedback gains at design condition

	Mach 0.9		Mach 0.7	
No.	Real	Imaginary	Real	Imaginary
1	−8.795	57.707	−16.024	61.519
2	−8.795	−57.707	−16.024	−61.519
3	−45.161	86.456	−60.178	81.449
4	−45.161	−86.456	−60.178	−81.449
5	−10.700	180.513	−17.947	178.983
6	−10.700	−180.513	−17.947	−178.983
7	−13.653	264.689	−11.548	256.785
8	−13.653	−264.689	−11.548	−256.785
9	−15.314	373.445	−21.332	367.960
10	−15.314	−373.445	−21.332	−367.960
11	−56.098	0.0	−28.655	28.334
12	−56.708	0.0	−28.655	−28.334
13	−46.519	33.385	−44.465	0.0
14	−46.519	−33.385	−44.636	0.0
15	−57.629	0.0	−44.960	0.0

the 50% margin exhibit acceptable levels of rms control surface displacement and rate for gust disturbances. Table 1 lists the eigenvalues at the design condition for the open-loop system.

Zero-state weighting ($Q=0$) was selected initially since this yields a set of gains that are "cheapest" in terms of input amplitude.[11] Table 2 lists the closed-loop eigenvalues at the design condition. One sees that the effect of this control law is

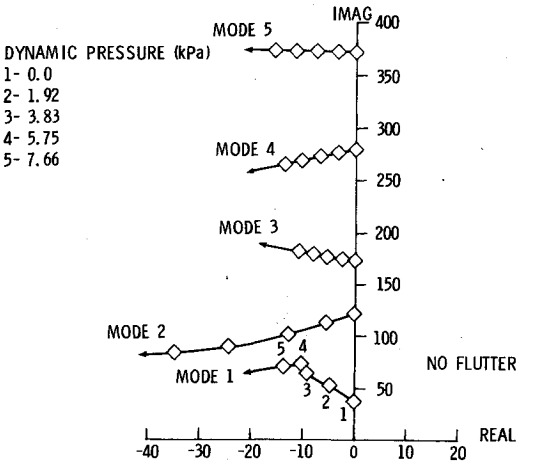

Fig. 5 Closed-loop $\bar{q}$ root locus using full-state feedback gains, Mach 0.9.

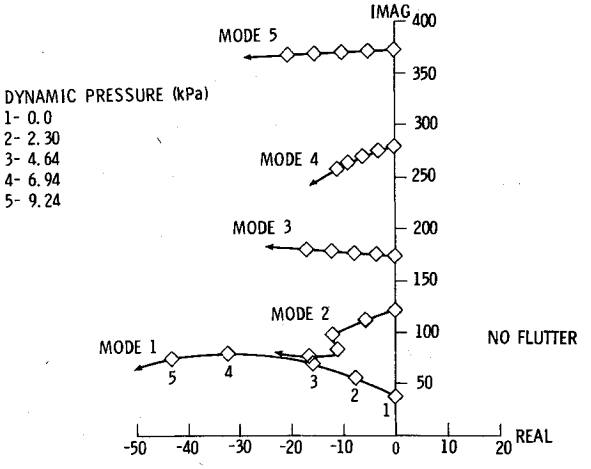

Fig. 6 Closed-loop $\bar{q}$ root locus using full-state feedback gains, Mach 0.7.

to leave all stable eigenvalues unchanged and reflect the unstable eigenvalues about the imaginary axis. Figures 5 and 6 show the root loci for the closed-loop system using the zero-state weighting gains. Flutter is not predicted within the range of dynamic pressures investigated (0-8.618 kPa). Figure 7 shows the control surface displacement and rate PSD at the Mach 0.9 design condition. The peak in the PSD is seen to be at the flutter frequency. Although the rms control rate is within an acceptable limit (211 deg/s/m/s), the rms control displacement (15.50 deg/m/s) is unacceptable. There is a similar result at Mach 0.7.

By studying the control law, it was determined that the gains on the generalized coordinate displacements are the major contributors to the large rms control displacements. Therefore, the gains on the displacements were set equal to zero and the stability characteristics were established at the design condition. Table 3 lists the closed-loop eigenvalues using the partial-state feedback. Although the damping in the flutter mode is reduced from $\zeta=0.19$ to $\zeta=0.15$, this is still an acceptable value. Figures 8 and 9 show the root loci for the closed-loop system using the partial-state feedback. Figure 10 shows the control displacement and rate PSD at the Mach 0.9 design condition using the partial-state feedback. At Mach 0.9, the rms control displacement is reduced to an acceptable level of 4.95 deg/m/s. Although the rms control rate increases to 275.9 deg/s/m/s, this is still an acceptable level. There is a similar trend at Mach 0.7.

A study was made to examine the effect of the weighting matrices in the cost function on the rms control displacement.

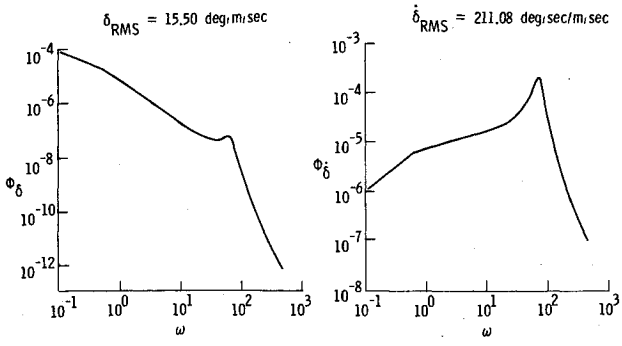

Fig. 7 δ and $\dot{\delta}$ PSD using full-state feedback gains at Mach 0.9 design condition.

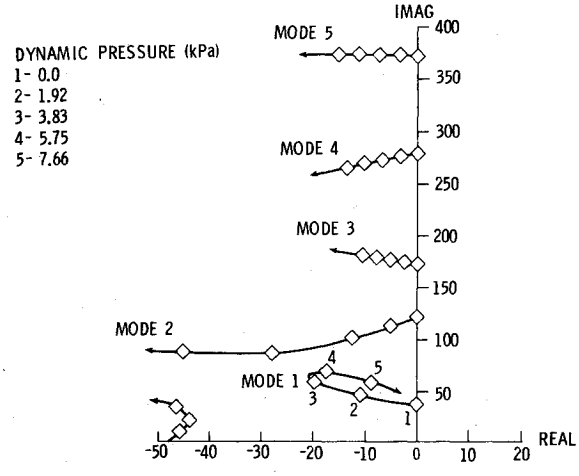

Fig. 8 Closed-loop $\tilde{q}$ root locus using partial-state feedback gains, Mach 0.9.

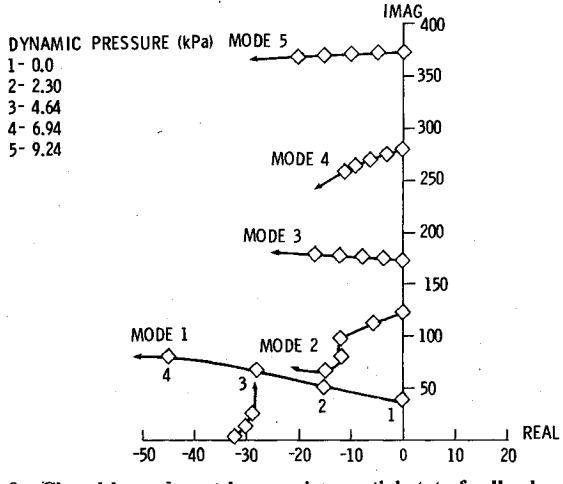

Fig. 9 Closed-loop $\tilde{q}$ root locus using partial-state feedback gains, Mach 0.7.

Figure 11 shows the effect of the control weighting matrix (R) on the rms control displacement. The state weighting matrix (Q) was held constant. The weight on the torsion mode was equal to 2×10^5 with the other terms equal to zero. This function was selected based on the two-dimensional results of Vepa.[5] The two curves in Fig. 11 show the effect of using the von Karman gust spectrum. A white-noise gust spectrum means that ϕw_g in Eq. (17) is equal to 1. The curve using the white-noise gust spectrum exhibits the behavior that is expected. The rms control displacement decreases as the control weighting matrix is increased. Using the von Karman

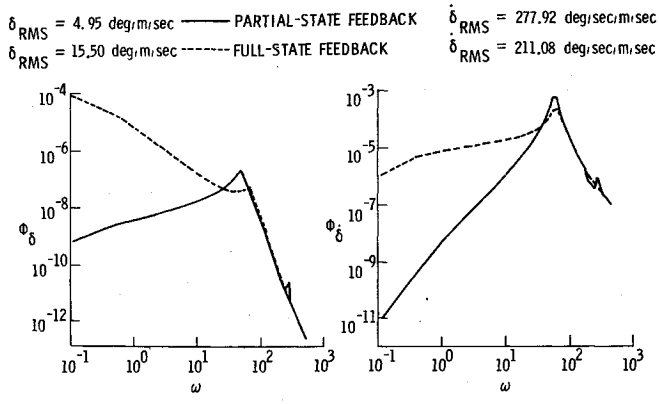

Fig. 10 δ and $\dot{\delta}$ PSD using partial-state feedback gains at Mach 0.9 design condition.

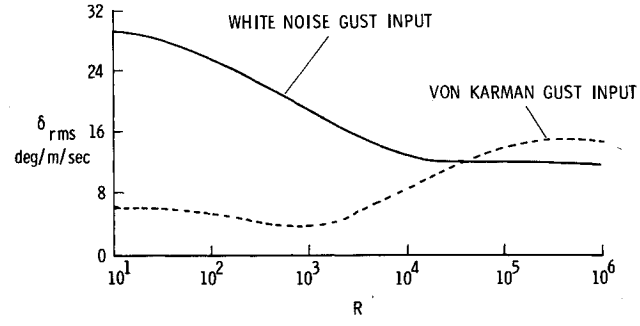

Fig. 11 δ_{rms} vs control weighting matrix with state weighting matrix constant at Mach 0.9 design condition.

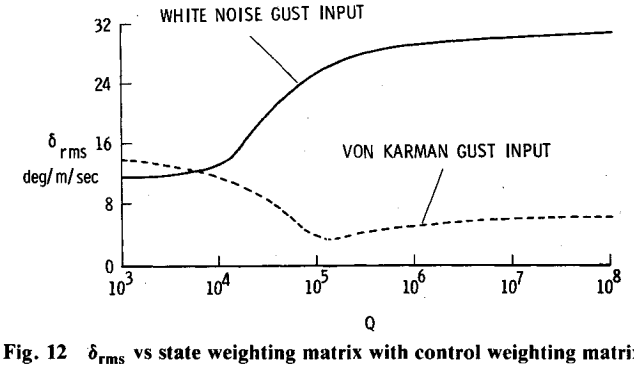

Fig. 12 δ_{rms} vs state weighting matrix with control weighting matrix constant at Mach 0.9 design condition.

gust spectrum, the rms control displacement shows a minimum at $R=10^3$. Figure 12 shows the same trend as was indicated in the previous figure. Using the von Karman gust spectrum, the rms control displacement shows a minimum of 3.66 deg/m/s at $Q=1.5\times10^5$.

Conclusions

Study results were presented demonstrating the use of optimal control theory for the synthesis of an active flutter-suppression control law. Numerical studies were conducted for a high-aspect-ratio wind-tunnel wing model. The numerical results indicated that the flutter dynamic pressure could be increased at least 50% using full-state or partial-state feedback. Although the rms control surface displacement due to gust disturbances at the design condition was very large when using full-state feedback, this could be reduced significantly by deleting the gains on the generalized coordinate displacements. Although this study only considered theoretical (i.e., state) feedback control laws, research in the areas of Kalman filtering and other methods for synthesizing

practical control laws for active flutter suppression using optimal control theory is underway.

Acknowledgments

This work was performed while the author was an employee of the Vought Corporation, Hampton Technical Center, and was sponsored by the National Aeronautics and Space Administration under Contract NAS1-13500. The work also constitutes a part of the author's M.S. Thesis at the George Washington University.

References

[1]Thompson, G.O., "Active Flutter Suppression – An Emerging Technology," *Journal of Aircraft,* Vol. 9, March 1972, pp. 230-235.

[2]Vepa, R., "On the Use of Padé Approximants to Represent Unsteady Aerodynamic Loads for Arbitrarily Small Motions of Wings." AIAA Paper 76-17, 1976.

[3]Edwards, J.W., "Unsteady Aerodynamic Modeling and Active Aeroelastic Controls," NASA CR-148019, 1977.

[4]Morino, L., "A General Theory of Unsteady Compressible Potential Aerodynamics," NASA CR-2464, 1974.

[5]Vepa, R., "Finite-State Modeling of Aeroelastic Systems," Ph.D. Dissertation, Department of Applied Mechanics, Stanford University, June 1975.

[6]Bisplinghoff, R., Ashley, H., and Halfman, R., *Aeroelasticity,* Addison Wesley Publishing Company, Reading, Mass., 1957, p. 555.

[7]Sandford, M.C., Abel, I., and Gray, D.L., "Development and Demonstration of a Flutter-Suppression System Using Active Controls," NASA TR R-450, Dec. 1975.

[8]Albano, E. and Rodden, W.P., "A Doublet-Lattice Method for Calculating Lift Distributions on Oscillating Surfaces in Subsonic Flows," *AIAA Journal,* Vol. 7, Feb. 1969, pp. 279-285.

[9]Giesing, J.P., Kalman, T.P., and Rodden, W.T., "Subsonic Unsteady Aerodynamics for General Configurations," AFFDL-TR-71-5, Nov. 1971.

[10]Sevart, F.D., "Development of Active Flutter-Suppression Wind-Tunnel Testing Technology," AFFDL-TR-74-126, 1975.

[11]Kwakernaak, H. and Sivan, R., *Linear Optimal Control Systems,* John Wiley and Sons, Inc., New York, 1972, p. 289.

[12]Houbolt, J.C., Steiner, R., and Pratt, K.G., "Dynamic Response of Airplanes to Atmospheric Turbulence Including Flight Data on Input and Response," NASA TR R-199, 1969.

[13]Perry B., "An Analytical Study of Turbulence Responses, Including Horizontal Tail Loads," M.S. Thesis, School of Engineering and Applied Science, George Washington University, Feb. 1976.

[14]Abel, I., Perry, B., and Murrow, H.N., "Synthesis of Active Controls for Flutter Suppression on a Flight Research Wing," AIAA Paper 77-1062, Aug. 1977.

[15]Visor, O.E. and Sevart, F.D., "Preliminary Design Study of a Flutter-Suppression Control System for the BQM-34E/F Drone Aircraft with a Supercritical Wing – Final Report," NASA CR-143208, 1978.